Science Advances
AAAS

advances.sciencemag.org/cgi/content/full/6/20/eaba1590/DC1

# Supplementary Materials for

## Bioinorganic hybrid bacteriophage for modulation of intestinal microbiota to remodel tumor-immune microenvironment against colorectal cancer

Xue Dong, Pei Pan, Di-Wei Zheng, Peng Bao, Xuan Zeng, Xian-Zheng Zhang*

*Corresponding author. Email: xz-zhang@whu.edu.cn

Published 15 May 2020, *Sci. Adv.* **6**, eaba1590 (2020)
DOI: 10.1126/sciadv.aba1590

**This PDF file includes:**

Figs. S1 to S9

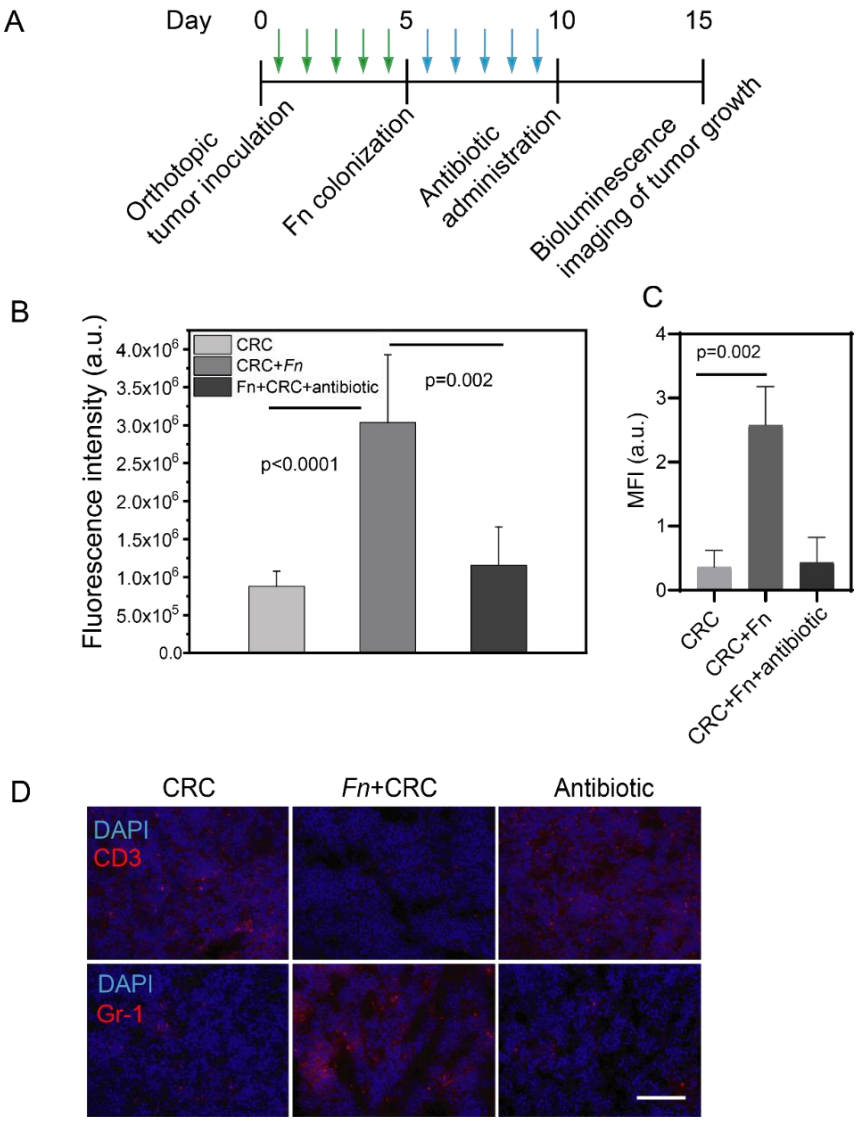


**Fig. S1. Effect of *Fn* in the CRC immune microenvironment.** (A) Schematic of treatment antibiotic on orthotopic CRC mice. (B) The corresponding quantitative evaluation for bioluminescence imaging of orthotopic CT26-luc tumor bearing mice with different treatments at 15 days (n = 5). (C) The corresponding quantitative evaluation for FISH staining of *Fn* after different treatments at 15 days. (D) Representative immunofluorescence staining images for CD3 and Gr-1 of tumor tissues in orthotopic CRC model after various treatments. (Scale bar: 200 μm). Significant difference was assessed in (B) and (C) by using t test. The mean values and S.D. are presented.

A

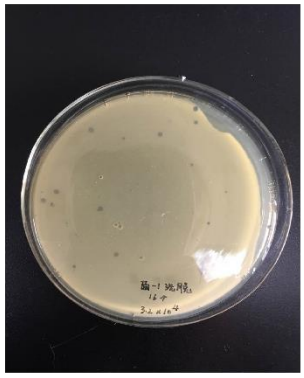

B

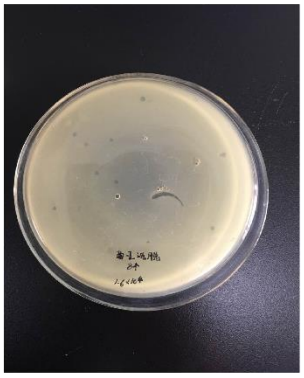

C

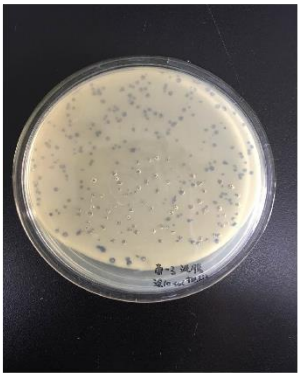

D

GTCCCACAATGGAAATTATTTTATTGACGAGCTCCGCCAGTATTGGAACGATATCAGGTCTACA
TTACTATTACCCCTCTTGCAACCTTCTTTGGCAAAAGCCTCTCGCTATTTTGTTTTATCGTCGTC
TGGTAAACGAGGGTATGATAGTGTGCTCTACTATGCTCGTAATCTTTTTGGCGTATGTATCTGC
ATTAGTGAATGTGGTATTCCTAAATCTCACTGATGAATCTTTCTACCTGTAATAATGTTGTTCCG
TTAGTTCGTTTTATTAACGTAGATTTTTCTTCCCAACGTCCTGACTGGTATAATGAGCCAGTTCT
TAAAATCGTATAAGGTAATTCACAATGATTAAAGTTGAAATTAAACCATCTCAAGCCCAATTTACT
ACTCGTTCTGGTGTTTCTCGTCAGGGCAAGCCTTATTCACTGAATGAGCAGCTTTGTTACGTT
GATTTGGGTAATGAATATCCGGTTCTTGTCAAGATTACTCTTGATGAAGGTCAGCCAGCCTATG
CGCCTGGTCTGTACACCGTTCATCTGTCCTCTTTCAAAGTTGGTCAGTTCGGTTCCCTTATGA
TTGACCGTCTGCGCCTCGTTCCGGCTAAGTAACATGGAGCAGGTCGCGGATTTCGACACAAT
TTATCAGGCGATGATACAAATCTCCGTTGTACTTTGTTTCGCGCTTGGTATAATCGCTGGGGGT
CAAAGATGAGTGTTTTAGTGTATTCTTTTGCCTCTTTCGTTTTAGGTTGGTGCCTTCGTAGTGG
CATTACGTATTTTACCCGTTTAATGGAAACTTCCTCATGAAAAAGTCTTTAGTCCTCAAAGCCT
CTGTAGCCGTTGCTACCCTCGTTCCGATGCTGTCTTTCGCTGCTGAGGGTGACGATCCCGCA
AAAGCGGCCTTTAACTCCCTGCAAGCCTCAGCGACCGAATATATCGGTTATGCGTGGGCGAT
GGTTGTTGTCATTGTCGGCGCAACTATCGGTATCAAGCTGTTTAAGAAATTCACCTCGAAAGC
AAGCTGATAAACCGATACAATTAAAGGCTCCTTTTGGAGCCTTTTTTTTGGAGATTTTCAACGT
GAAAAAATTATTATTCGCAATTCCTTTAGTGGTACCTTTCTATTCTCACTCTTTTACTCTTCCGC
GGCTGAATCTTGCGATGATTGCTGGTGGAGGTTCGGCCGAAACTGTTGAAAGTTGTTTAGCA
AAATCCCATACAGAAAATTCATTTACTAACCGTTCTGAAAAGGCCGCCCAAT

**Fig. S2. Screening and identification of M13@Ag to specifically elimination of *Fn*.** Typical images of double-layered plate with specifically *Fn*-binding M13 phages: (A) The first round of screening. (B) The second round of screening. (C) The third round of screening. (D) Genome information of M13 phage named M5 from a phage display library by high-throughput sequencing. (Photo credit: Xian-Zheng Zhang, Wuhan University).

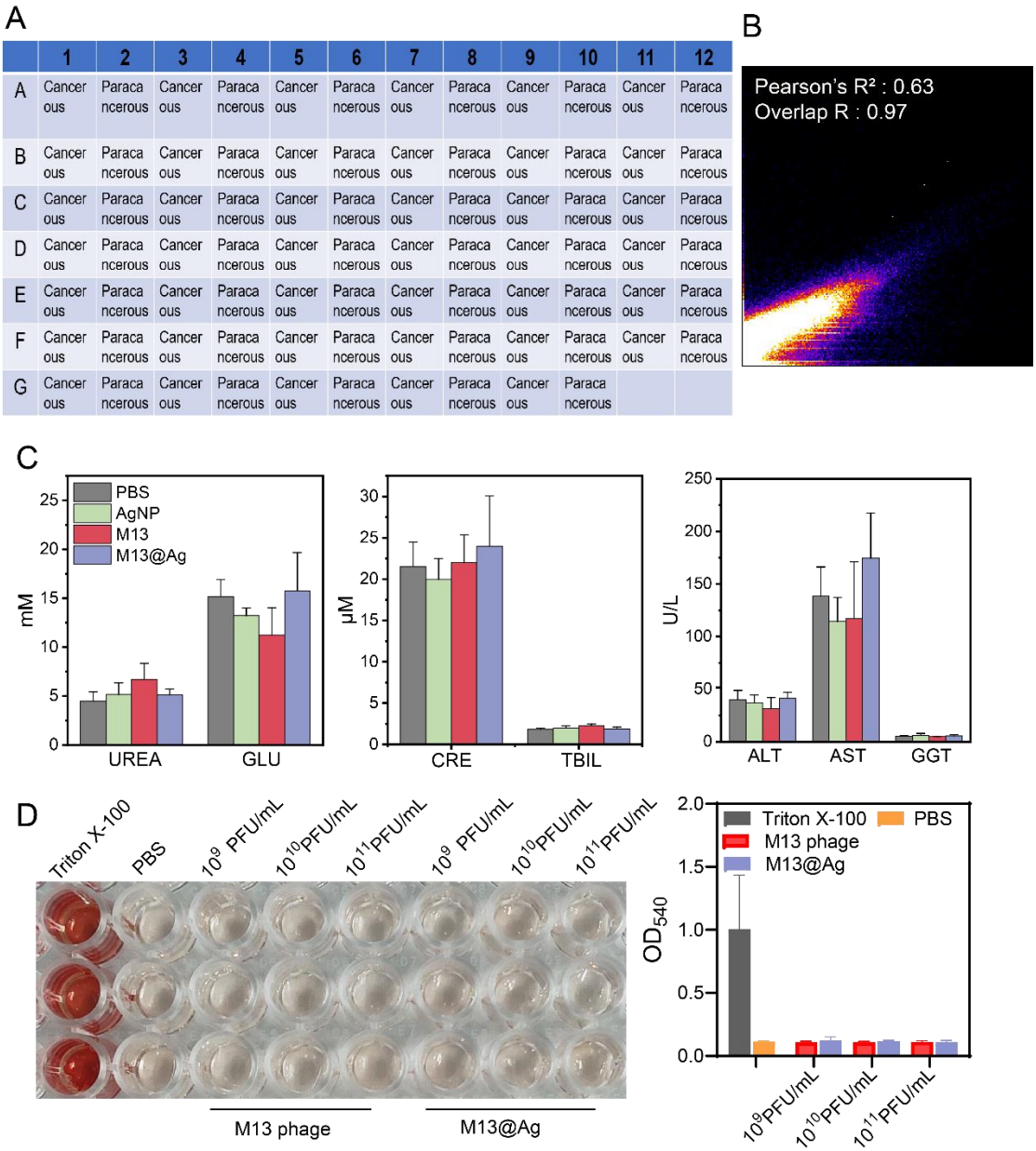


**Fig. S3. Information of the tissue sample and biosafety of M13@Ag.** (A) Sample information of tissue microarray. (B) Fluorescence co-localization analysis of *Fn* and MDSCs in clinical tumor samples. (C) The blood biochemistry of BALB/c mice after different treatments (n = 4). (D) The hemolytic test after different concentration M13@Ag treatments (n = 3). (Photo credit: Xian-Zheng Zhang, Wuhan University).

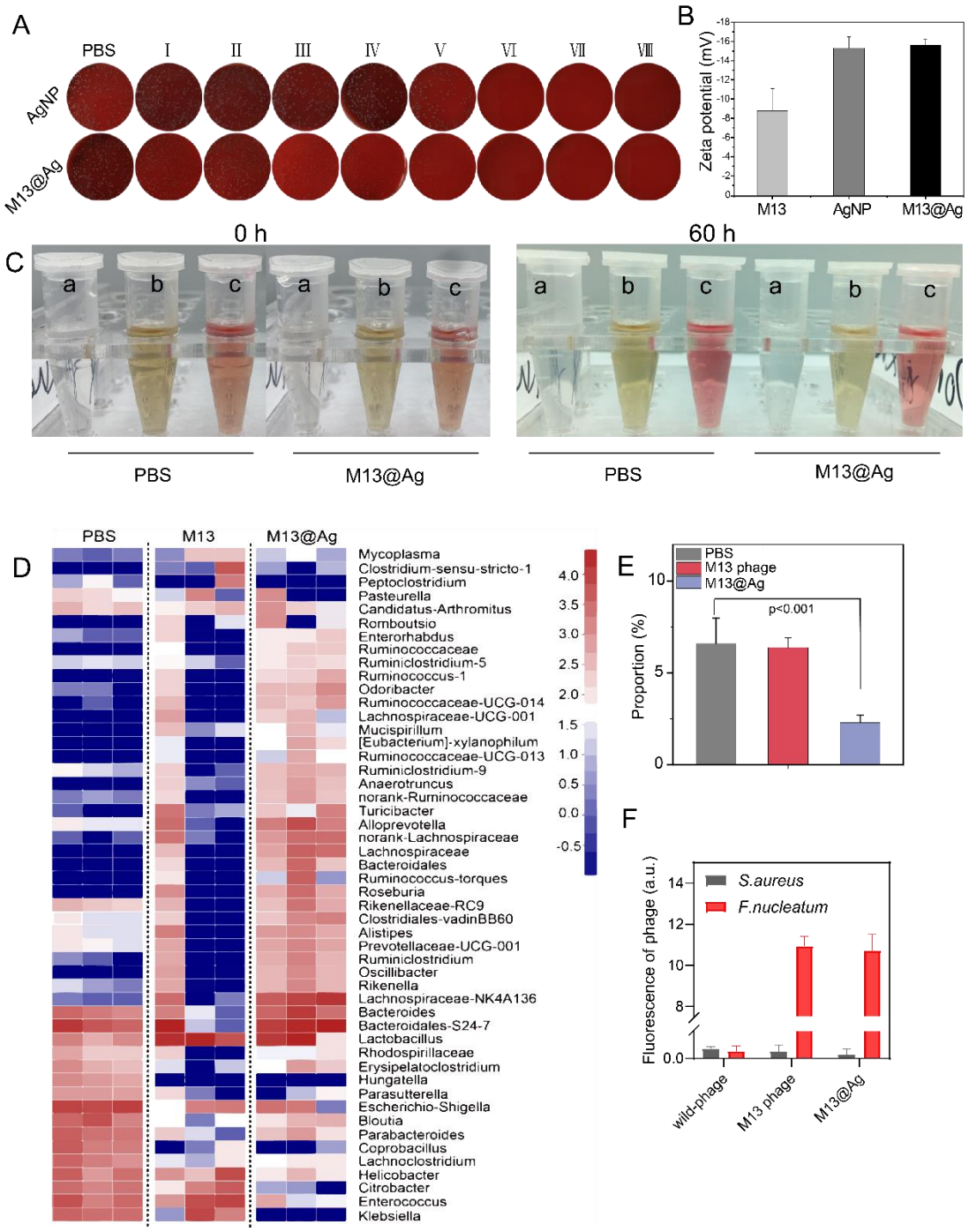


**Fig. S4. Capacity of anti-bacteria and regulate gut microbiota after M13@Ag treatment.** (A) Bacterial colony of *Fn* incubated with AgNP and M13@Ag. I-VIII were represented different concentrations of Ag. I: $5\times10^{-4}$ μg/mL; II: $2\times10^{-3}$ μg/mL; III: 0.01 μg/mL; IV: 0.06 μg/mL; V: 0.29 μg/mL; VI: 1.44 μg/mL; VII: 7.2 μg/mL; VIII: 36 μg/mL. (B) Zeta potentials of M13 phage, AgNP and M13@Ag. (C) Stability test of M13@Ag resuspended in PBS (a), serum (fetal bovine serum (FBS), b) and cell culture media (DMEM, c). (D) Community heatmap of fecal microbiota

compositions in PBS, M13 phages and M13@Ag treated *Fn*-colonized CRC murine model (n = 3). (E) qPCR analysis level of *Fn* in fecal samples after treatments (n = 3). (F) Quantitative analysis of red fluorescence (M13 phage) in phage-binding assays *in vitro*. Significant difference was assessed in (B) by using t test. The mean values and S.D. are presented. (Photo credit: Xian-Zheng Zhang, Wuhan University).

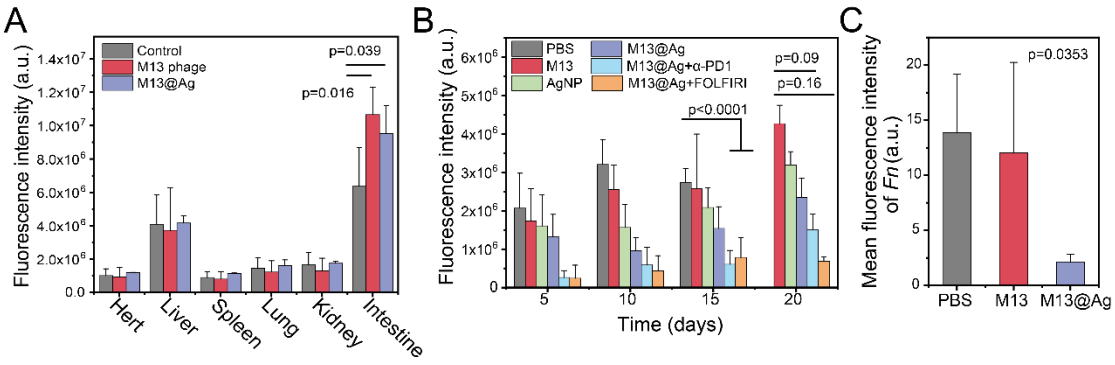


**Fig. S5. *In vivo* tumor targeting and tumor treatment capacity of M13@Ag.** (A) The quantitative evaluation for *ex vivo* fluorescence imaging of the major organs in orthotopic CRC mice model after injection of wild-type phage, M13 phages and M13@Ag at 24 h (n = 3). (B) The corresponding quantitative *in vivo* bioluminescence imaging of orthotopic CT26-luc tumor bearing mice during the receiving treatments (n = 5). (C) Quantitative analysis for mean fluorescence intensity of FISH staining of *Fn* after PBS, M13 phages and M13@Ag treatments. Significant difference was assessed in (A) and (B) by using t test. Significant difference was assessed in (C) by using one-way ANOVA. The mean values and S.D. are presented.

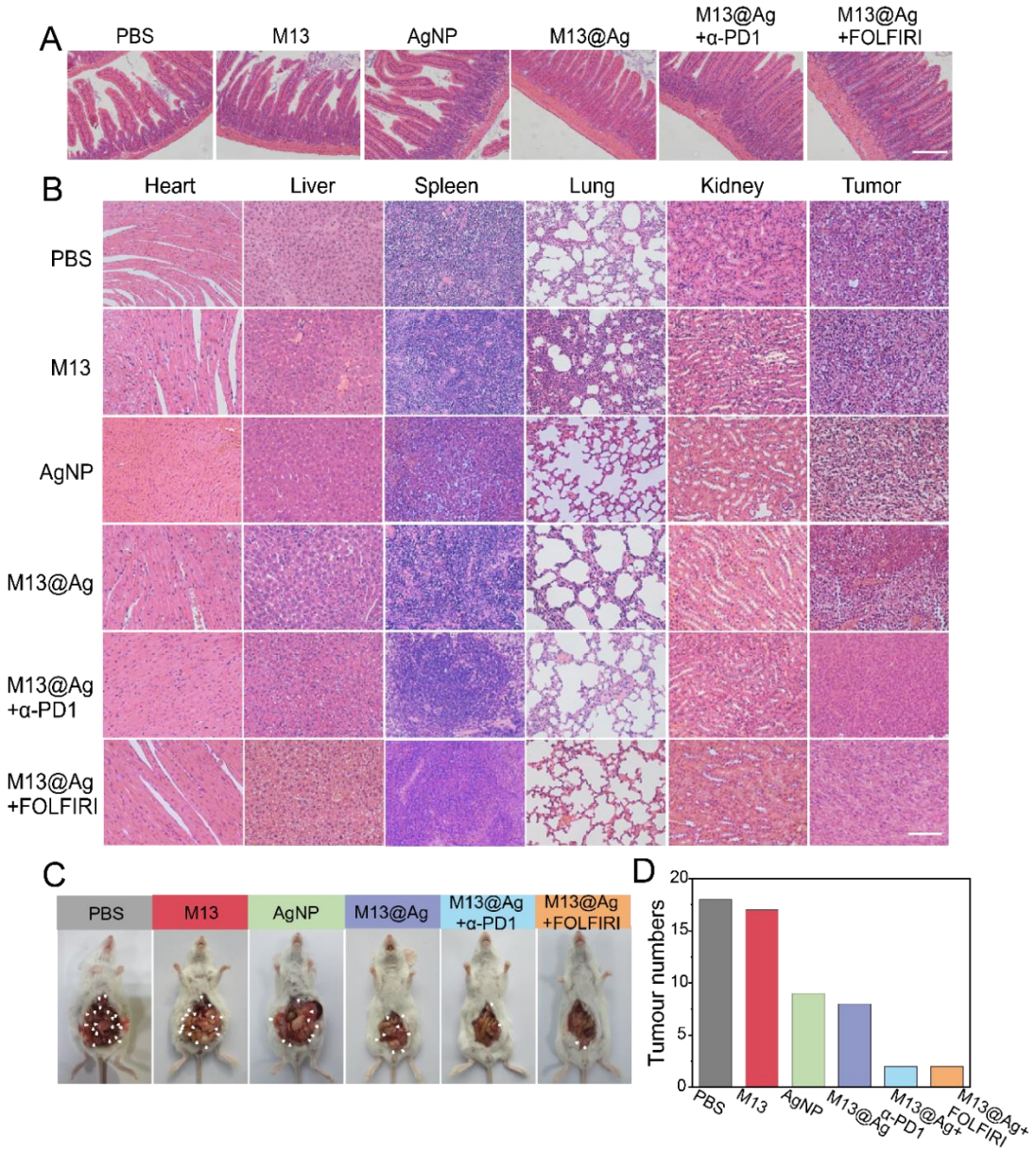


**Fig. S6.** ***In vivo*** **therapeutic effect of M13@Ag in orthotopic CT26-luc tumor mode.** (A) H&E staining of colon cancer tissues in PBS, M13, AgNP, M13@Ag, M13@Ag + α-PD1 and M13@Ag + FOLFIRI treated mice. The intestinal mucosa of orthotopic CT26-luc tumor bearing mice that received M13@Ag + α-PD1 and M13@Ag + FOLFIRI treatments showed longer and regular villi (Scale bar: 400 μm). (B) H&E staining of the major organs (heart, liver, spleen, lung and kidney) in orthotopic CT26-luc tumor bearing mice after different treatments (Scale bar: 200 μm). (C) Representative images of colon tumors in orthotopic tumor bearing mice. (D) The numbers of abdominal tumor metastasis after various treatments. (Photo credit: Xian-Zheng Zhang, Wuhan University).

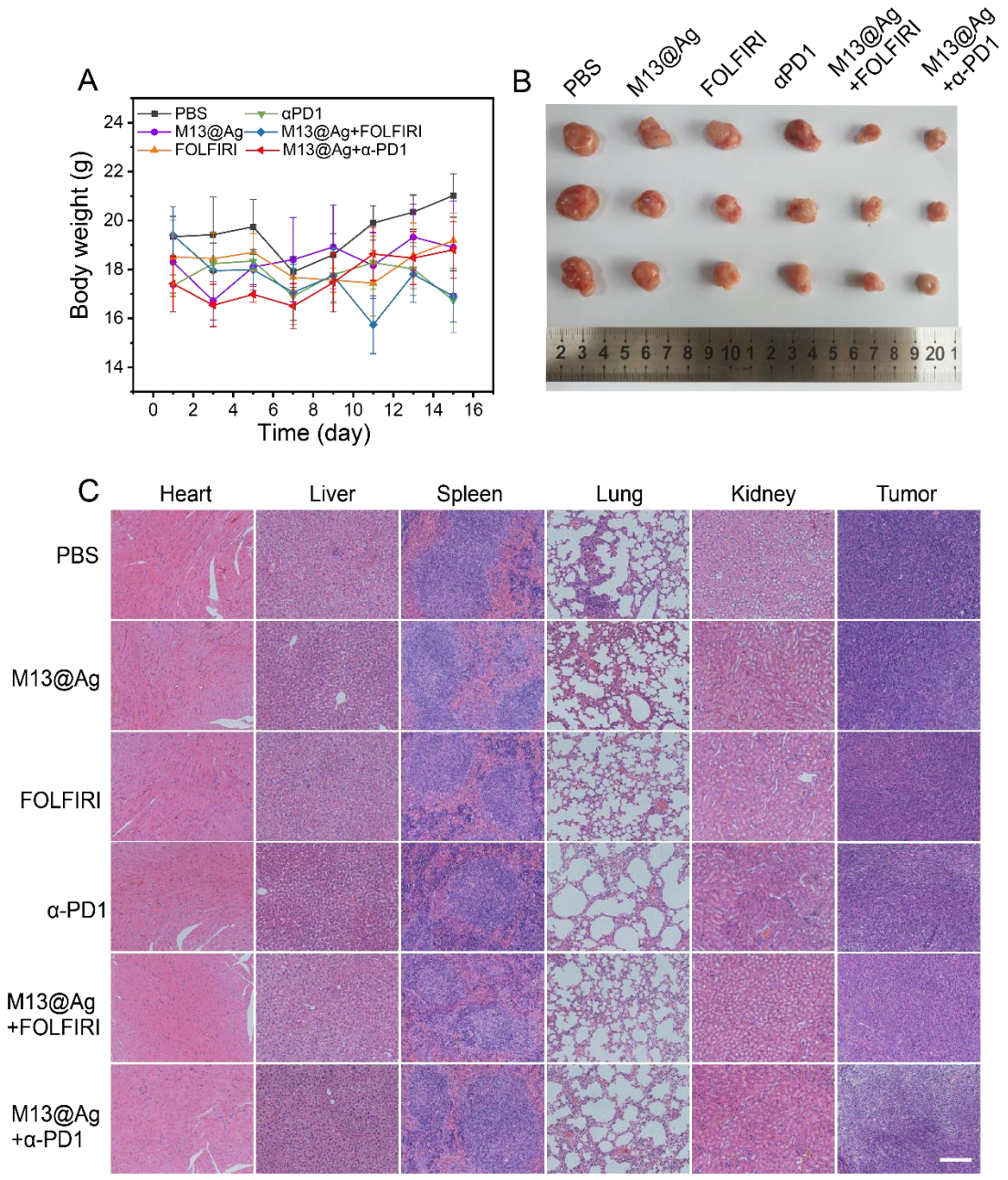


**Fig. S7. *In vivo* therapeutic effect of M13@Ag in subcutaneous CT26 tumor mode.** Relative body weight (A) and representative image of tumor tissues (B) harvested from different groups in subcutaneous CT26 tumor mode after various treatments (n = 5). (C) H&E staining of the major organs (heart, liver, spleen, lung and kidney) in subcutaneous CT26 tumor mode at post treatment in 14 days (Scale bar: 200 μm). (Photo credit: Xian-Zheng Zhang, Wuhan University).

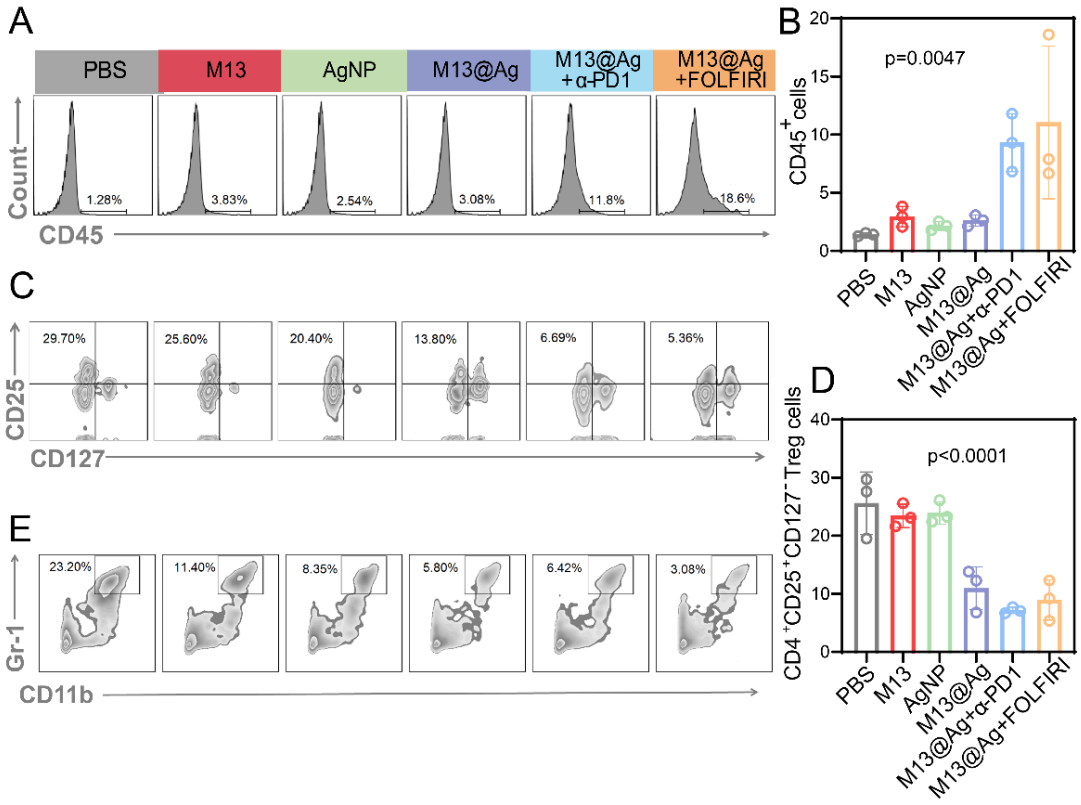


**Fig. S8. Flow cytometric analysis images and relative quantification in orthotopic CT26-luc tumors.** (A-B) Representative flow cytometric analysis images and quantification of $CD45^+$ lymphocytes. (C-D) Flow cytometric analysis of immunosuppressive $CD4^+CD25^+CD127^-$ Tregs in tumor tissues. (E) Representative flow cytometric analysis images of $CD11b^+$Gr-1 MDSCs in spleen (n = 3). Significant difference was assessed using one-way ANOVA. The mean values and S.D. are presented.

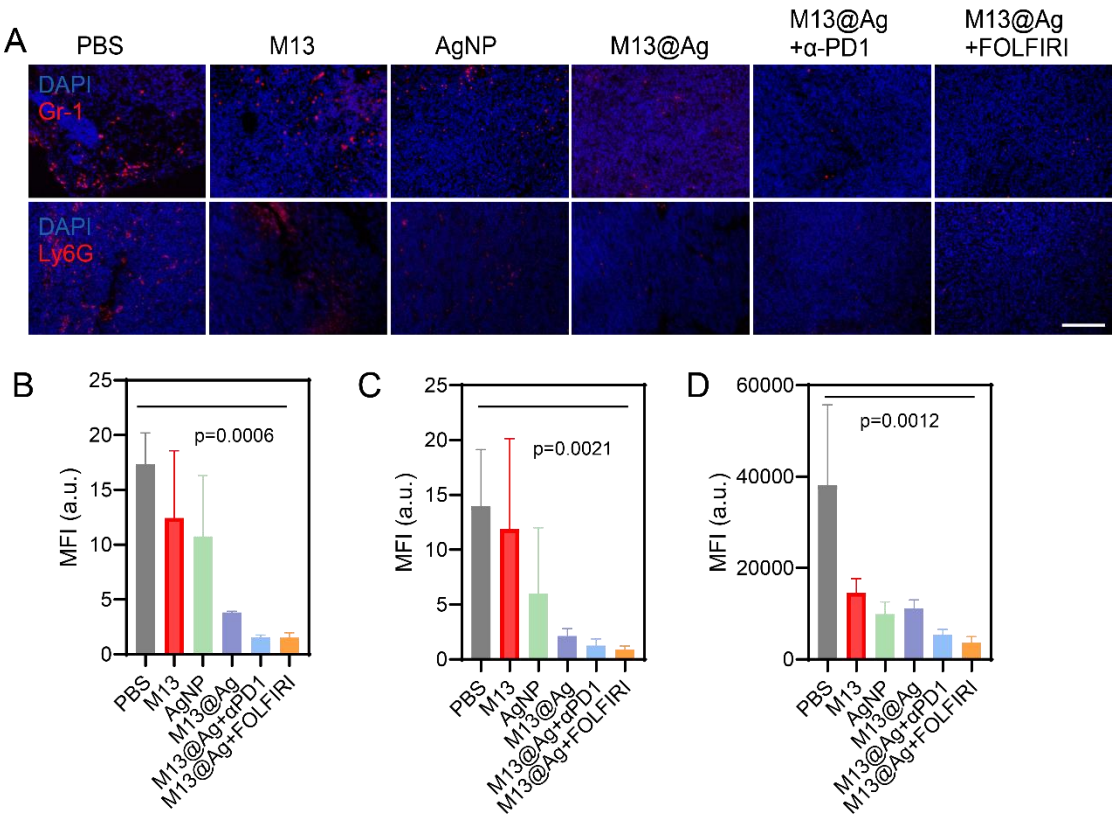


**Fig. S9. Representative images and quantification of immunofluorescence staining from orthotopic CRC tumor tissues.** (A) Representative immunofluorescence staining images for Gr-1 and Ly6G from orthotopic CRC tumor tissues at the 14th day post different treatments (Scale bar: 200 μm). (B-D) Quantification of representative images for Ki67, FISH and Arg-1.